Article:

Walker, C., Heitor, A. orcid.org/0000-0002-2346-8250 and Clarke, B. (2023) Impact of drying-wetting cycles on the small strain behaviour of compacted clay. Transportation Geotechnics, 42. 101063. ISSN 2214-3912

https://doi.org/10.1016/j.trgeo.2023.101063

Impact of drying-wetting cycles on the small strain behaviour of compacted clay

Author 1: Christopher Walker, MSc, PhD candidate

Department of Civil Engineering, University of Leeds, Leeds, UK

ORCID number: 0000-0002-4257-7794

Author 2: Ana Heitor, PhD , Lecturer

Department of Civil Engineering, University of Leeds, Leeds, UK

ORCID number: 0000-0002-2346-8250

Author 3: Barry Clarke, PhD , Professor

Department of Civil Engineering, University of Leeds, Leeds, UK

ORCID number: 0000-0001-9493-9200

Full contact details of corresponding author.

Ana Heitor

School of Civil Engineering, University of Leeds

Leeds, UK

Ph: +44 7849282475

Email: a.heitor@leeds.ac.uk

Submitted to: Transportation Geotechnics

Word count (excluding abstract and references):7360

No. of Figures: 15

No. of Tables: 3

Abstract (150 – 200 words)

Small strain shear modulus (G_{max}) is an important parameter for assessing the performance of compacted soils that underlie typical transport infrastructure assets such as railway tracks. This is particularly important when considering changes in climate patterns, which are expected to yield larger seasonal soil-atmosphere moisture fluctuations. This in turn results in the progressive variation of the small strain properties of compacted soils during their service life (i.e. drying and wetting). In this study, the small strain shear behaviour was evaluated for an intermediate plasticity clay (i.e. kaolin) in a series of drying and wetting cycles . Four different dying and wetting boundaries were considered to explore a wide range of moisture amplitudes during 10 drying-wetting cycles. Drying and wetting was controlled using gravimetric water content in order to mimic realistic field conditions typically observed at substructure level. An ultrasonic pulse transmission method was used to capture the change in small strain stiffness and volume at discrete points during the drying-wetting cycles. The results reveal clear distinctions in behaviour for all four boundaries considered, with wetting boundaries having the greatest influence on behaviour. In this instance, specimens brought to full saturation during wetting exhibited an increase in the small strain shear modulus during progressive drying-wetting cycles. However, a reduction was observed when the wetting boundary was restricted to the compacted state. Measured volume changes were also in agreement with these findings, however there was some evidence of volume increase when drying to residual conditions. The results suggest that this is associated with the formation of the partial pendular state where a loss of capillary contacts between particles occurs. Furthermore, when all data for 10 drying-wetting cycles is plotted in the e-G_{max} space, a linear relationship is observed for different constant water content levels. Remarkably, this trend is shown to be independent of the boundary conditions considered in this study or number of drying-wetting cycles.

Keywords

Drying-wetting cycles; small strain stiffness; compacted clay; ultrasonic pulse transmission testing; geostructures; amplitude of drying and wetting

1 Introduction

Compacted soils included in earth structures, such as transport infrastructure embankments, are exposed to a range of persistent cyclical oscillations in hydraulic loads resulting from soil-atmosphere interactions. The extent of these interactions results from the incidence of precipitation, relative humidity and surface temperature associated with prevailing weather conditions. In addition, they are also influenced by soil properties/features such as permeability, plasticity, particle size, desiccation cracking and presence of vegetation. These geomaterials are placed and compacted using plant (e.g. vibrating or sheep foot rollers) to a specified compaction criteria (e.g. dry unit weight and water content) and typically remain in an unsaturated condition during most of their service life, which governs their stress strain behaviour.

During the operation of transport infrastructure, the small strain (0.001% or less) properties of these geomaterials governs the response of an earth structure subjected to dynamic loading resulting from passing traffic. Historically, both field and laboratory shear wave testing techniques such as seismic cone penetration testing (SCPT) and bender element techniques have been used to measure small strain properties. These methods measure the propagation of shear waves, which travel transverse to the direction of transmission at a given frequency and amplitude, over a known distance to determine the velocity of the transmitted wave in either saturated or unsaturated conditions (Krautkrämer et al., 1990).

In unsaturated conditions the differential between soil water pressure and air pressure applies a tensile force at the air-water interface producing an additional normal stress (capillary stress as matric suction) between soil particles. Upon exceeding the Air Entry Value (AEV), the air phase becomes continuous in the pores and soil enters the transition zone. Generally, the associated increase in the magnitude of suction results in an increase in soil stiffness and thus small strain shear modulus ($G_{\max}$) (Ngoc, 2020). Consequently, the propagation of shear waves depends on void ratio, matric suction and net stress i.e. inter-particle forces (Cho and Santamarina, 2001; Whalley et al., 2012; Santamarina, 2003). Numerous past studies have demonstrated that the velocity of shear waves in soil, and thus small strain shear modulus is sensitive to soil water retention characteristics, for example, Azizi et al. (2019); Ngoc et al. (2019); Heitor et al. (2015b); Khosravi and McCartney (2012); Ng et al. (2009), among others. They report that small strain stiffness also exhibits hysteretic behaviour observed during drying and wetting resulting from the 'ink bottle effect' (distribution of pore size diameter) and differences in contact angles (Heitor, 2013). Past research by Ngoc et al. (2019) has also shown that van der Wall attraction (intermolecular force) and double-layer repulsion (formed at the soil-water interface) influences observed shear modulus during drying and wetting cycles.

Furthermore, the application of several drying-wetting cycles has also been shown to impact the small strain shear modulus of compacted soils (Ma, C. et al., 2023; Ying et al., 2021; Ngoc, 2020; Tang et al., 2011; Heitor et al., 2015b). For instance, Ying et al. (2021) and Tang et al. (2011) showed a slight decrease in small strain shear modulus for compacted sandy silts subject seven drying-wetting cycles. However both Ngoc (2020) and Heitor et al. (2015b) report increases in small strain shear modulus after drying-wetting cycles for compacted mixture of kaolin and sand, and silty sand respectively. As a result the behaviour of compacted soils has been shown to be complex however, there is no quantitative evidence explaining the causes of the difference in observed behaviour.

The consideration of these complexities is important with regard to future changes in climate which will likely alter the amplitude of hydraulic cycles experienced by compacted soils (Walker et al., 2022). Past studies have shown that the resultant predicted increase in climatic extremes generate higher suction stresses during hotter summer periods, leading to increased amplitude of water content during drying and wetting, and thus a greater volume change observed in the seasonal shrink-swell cycles (Clarke, D. and Smethurst, 2010; Glendinning et al., 2015). Recent research has also shown that continual drying and wetting processes also produce weather driven deterioration of the soil microstructure. This has been shown to result from the formation of micro-cracks which propagate during hydraulic cycling in the surface of an embankment (Stirling et al., 2020). Triaxial testing demonstrated that this mechanism produced an asymptotic reduction in shear strength of a glacial till at large strains. The observed change in strength reached an equilibrium after several cycles and is presumably as a result of changes in the soil microstructure (Stirling et al., 2020). However, the impact of hydraulic pathways, such as differing drying-wetting amplitudes and boundaries relevant to climate change have not been investigated for compacted clay soils.

This paper therefore examines the effect of drying and wetting cycles on the shear modulus of compacted kaolin clay measured using ultrasonic testing techniques. Four hydraulic amplitudes were investigated incorporating the complete range of the soil water retention curve (SWRC). This is contextualised with reference to climate change and includes salient variables regarding drying and wetting boundaries. Specimens were subjected to ten drying and wetting cycles within these defined parameters. Furthermore, unlike previous studies on small strain stiffness, the hydraulic cycles (drying and wetting) were controlled using gravimetric water content rather than adopting constant suction levels via the axis translation technique. This approach allowed for saturation and suction to remain dependent variables during application of hydraulic cycles, thus simulating field conditions more closely.

2 METHODOLOGY

2.1 Materials and specimen preparation

Laboratory testing was conducted on commercial kaolin clay procured from Imerys Ltd. The material is characterised by a plasticity index of 23%, a liquid limit of 56% and specific gravity 2.61 (Table 1). The particle size distribution of the sample includes 62% fine and medium silt and 38% clay size fraction (Figure 1). In this study, kaolin clay was selected because its behaviour and properties (i.e. compacted pore size distribution) have been well characterised by several past studies (Tarantino and Col, 2008; Tarantino and Tombolato, 2005; Vesga, 2008; Thom et al., 2007; González and Colmenares, 2006). Furthermore, kaolin clay is an intermediate plasticity clay which is representative of several soils in the UK, for example Weald clay and matrix-dominated tills (Reeves et al., 2006; Clarke, B.G., 2018).

The specimens were statically compacted using a split mould to a desired dry unit weight by applying a constant force. Similar procedures have been adopted in several past studies; for example Azizi et al. (2018); Reddy and Jagadish (1993); Tarantino (2009); Tarantino and Col (2008), among others. This method minimises disturbance resulting from sub sampling and thus maintains higher repeatability and precision between specimen compaction conditions.

The dry powdered kaolin was mixed with demineralised water to achieve the required water content prior to compaction. The material was then passed through a 2 mm aperture sieve to reduce the size of aggregated particles. The wet kaolin sample was sealed and kept at approximate constant temperature and humidity conditions for a minimum of 24 hours to ensure moisture equilibration. Specimens were statically compacted using a static stress level of 1400 kPa to a diameter of 38 mm and height of 76 mm. To minimise friction, dry Polytetrafluoroethylene (PTFE) was used to coat the split mould walls and soil was compacted in two layers. Each layer was statically compacted at a constant force for 1 hour to reach maximum volume change. After placement of the first layer, the surface was scarified to ensure good adhesion between both layers.

A comparison between the compaction behaviour statically achieved in the split moulds and the standard Proctor test is shown in Figure 2 (BS 1377-2:2022). Results show that static compaction achieved 93% of standard Proctor maximum dry unit weight when a static stress of 1400 kPa was applied at the Proctor optimum moisture content (OMC). This represents a compaction level which is greater than the lower end of compaction criteria applied in the field (90%-95%) according to National Highways specifications (National Highways, 2016). Table 1 shows a summary of the selected specimen conditions.

The water retention characteristics were also determined for the statically compacted kaolin using the filter paper method. In this study, several specimens were wetted or dried to reach selected water contents following compaction so that a good breath of suction values were obtained. The filter paper method was then conducted using Whatman grade 42 filter paper in accordance with ASTM D5298-10 (2010). A minimum period of 7 days was adopted for equilibration of the test specimens. Matric suction was determined using contact method and calculated using the calibration curves reported by Leong, E.C. and Rahardjo (2002). The soil water retention curve (SWRC) was then interpolated using the close form relationship proposed by Genuchten (1980). The SWRC for compacted kaolin used in this study is shown in Figure 3.

2.2 Ultrasonic testing and small strain shear modulus

Ultrasonic testing is a non-destructive method which uses ultrasonic waves with a frequency above audible sound between 20 kHz and 1 GHz (Leong, E. et al., 2011). Similar to bender element tests, piezoelectric crystals are excited to produce motion and propagate an ultrasonic wave through a specimen. However, unlike bender elements the ceramic piezoelectric crystals are bonded to a platen rather than placed in direct contact with a material. An acoustic couplant was therefore used to displace the air and reduce the difference in acoustic impedance between the transducers and the soil to ensure good contact between the platen and the specimen. This method therefore does not require specimen protrusion and disturbance is kept to a minimum (Cheng and Leong, 2014).

In this study, the Pundit Lab testing system generated the electrical input signal consisting of 2 V. An Olympus contact transducer (V150-RB) converted the electrical input pulse into mechanical energy (transmitter) and a second corresponding transducer with a matching orientation acted as a receiver for the wave. Both compressional and shear waves can be monitored with this system. A digital oscilloscope connected to a PC then displayed both the input and received waves for analysis. The device displays a 12 bit resolution and 500 kHz sampling rate to ensure an adequate resolution in the time domain. The diagram of the experimental setup during capture of shear wave data is shown in Figure 4.

A square impulse was used as the input signal. A range of input wave frequencies were tested, i.e. 24 kHz, 37kHz, 82 kHz, 150 kHz, 200 kHz 220 kHz and 250 kHz. Figure 5 shows a typical time domain plot of a received wave for kaolin statically compacted at 28% water content.

Selecting adequate testing variables including the testing frequency is important for determining the correct wave velocities. Pulse transmission results for a compacted silty sand reported by Heitor et al. (2015b) show that at low frequencies the impact of the near field effect increases the travel times, and thus generate the risk of underestimating the shear wave velocity. In this study, observation of received waveforms collected from frequencies ranging from 24 kHz to 250 kHz showed approximately equal travel times (Figure 5). Arulnathan et al. (1998) proposed L_{pp}/λ >2 (L_{pp} platen-to-platen length), a ratio of wavelength and wave path, to minimise the impact of the near field effect. However, use of the 24 kHz frequency yields a L_{pp}/λ ratio of 7.0 at the compacted water content whereas 250 kHz frequency produces a L_{pp}/λ ratio of 72.7. Furthermore, consideration is required for L_{pp}/λ during drying and wetting as both the wave path and length are altered due to variation in shear wave velocity and specimen height. Results of an assessment of its effect on a compacted kaolin specimen presented in Table 2 show that following drying to 1.5% water content an approximate 35% reduction of the L_{pp}/λ ratio occurs for both 24 kHz and 250 kHz. However, at 1.5% water content a 24kHz frequency generates a value of L_{pp}/λ >2. Thus, the impact of the near field effect is minimal during drying-wetting using ultrasonic equipment. As a result, the selected frequency during testing does not significantly impact the arrival time. Testing was therefore conducted at various frequencies, selected depending on the amplitude of the received wave and suitable identification of the wave arrival (i.e. higher frequencies reduce wave intensity and thus decrease definition of the wave arrival).

Waveforms were interpreted using time domain method whereby the shear wave velocity was determined from the interval between the input wave and its first arrival by visual selection. The initial platen-to-platen distance was determined based on the total height of the specimen. The travel time of the shear wave was taken at the first deflection where the signal crossed the abscissa for repeatability. One of the difficulties when employing the time domain method is the presence of reflected or refracted compressional waves, which mask the first arrival of the shear wave (Da Fonseca et al., 2009). These challenges have been reported by Cheng and Leong (2014) for kaolin samples where a stronger compression wave component, delivered with eight times the intensity, masked the shear wave arrival. Figure 5 shows an example of the earlier arrival of a compressional wave during testing on the statically compacted kaolin specimens used in this study. Lee and Santamarina (2005) also reported similar observations for both partially saturated and unsaturated specimens. However, Figure 5 shows a clear distinction between the compression and shear wave arrival time in the time domain due to their contrasting amplitudes. The ability to successfully detect the shear wave arrival for kaolin specimens using ultrasonic transducers is also reported by Leong, E. et al. (2011) and Nakagawa et al. (1996). The difference in reported findings for its detection results from variation in specimen conditions (compaction/consolidation stress, saturation, confining stress, sample length) and configuration of transducers.

To calibrate the transducers, face-to-face tests were used to determine the delay calibration time (D). This accounts for the delay of the propagating incident wave as it travels through the platen and the shear wave couplant. In this method the delay is measured from the offset of the received wave from the transmitted wave when both transducers are in contact. The chosen method returned a delay calibration time (D) of approximately 2.4 μs, which was applied to all subsequent measurements. Other methods proposed for calibration include, measurement of the pulse travel time in a material of various lengths (obtaining the y-axis intercept when length is plotted against arrival time) and use of materials of known shear wave velocities (Leong, E. et al., 2011).

When using pulse transmission tests the consideration of the differences in the impedance of measured materials is important due to the attenuation of the input signal. For instance, when two materials such as the transducer platen and soil surface adhere to one another, the incident wave will propagate to the latter as a transmission wave. However, the difference in acoustic impedance of the two materials results in reflection of a portion of the incident wave sound pressure when the boundary is assumed perpendicular and smooth (Krautkrämer et al., 1990). When making these assumption determination of the percentage of energy transmitted to the soil can be achieved by calculation of the acoustic impedance (Z) as follows:

$$Z = \rho V \tag{1}$$

Where Z is the acoustic impedance (kg/m^{2}s), ρ is the density (kg/m^3) and V is the sound velocity (m/s). The reflection at the boundary can then be calculated using:

$$R = \left[\frac{(Z_t - Z_s)}{(Z_t + Z_s)}\right]^2 \tag{2}$$

Where Z is again the impedance and subscripts represent the transducer (Z_t) and specimen (Z_s). For the purpose of the calculation in this study a platen impedance equal to aluminium was assumed (Cheng and Leong, 2014). The results in Table 3 show that 81% of the shear wave is reflected at the soil-platen boundary. However, compressional wave reflectance was much greater clarifying the observed difference in compressional and shear wave amplitudes in the time domain. Cheng and Leong (2014) also reported similar wave transmission data for consolidated kaolin slurried at 100 kPa. They observed reflection of 88% of the incident sound pressure for both the shear and compression waves. Concluding it to be the partial cause of the masking of the shear wave arrival. After interpretation of the waveforms, the shear wave velocity (V_s) is determined, as follows:

$$V_s = \frac{L_{pp}}{\Delta t_s - D} \tag{3}$$

Where L_{pp} is the wave path length, which is determined from the distance between platens, Δt_s the travel time of the shear wave and D the delay calibration. The small strain shear modulus can be evaluated using:

$$G_{max} = \frac{\gamma_b}{g} V_s^2 \tag{4}$$

Where, γ_b is the bulk unit weight (kN/m³), g is acceleration due to gravity and V_s is the measured shear wave velocity.

2.3 Testing Programme

Climate change is expected to alter the amplitude of hydraulic cycles experienced by compacted soils used in transport infrastructure in the UK (Walker et al., 2022). UKCP18 predicts increases in future surface temperatures and the frequency and intensity of rainfall and flooding (Lowe et al., 2019). Modelling by Clarke, D. and Smethurst (2010) (using UKCP09 medium high emission scenario data) showed that predicted increases in the UK summer temperatures will result in a corresponding increase in soil moisture deficits by 2080 in compacted London clay fills. However, the impact of this predicted change on compacted soils has not been reported. Therefore in this study, the extent of the hydraulic cycle (i.e. range of drying and wetting) forms the independent variable from which the change in small strain behaviour was observed.

The initial dimensions, compaction stress and water content were maintained as constant variables for each specimen. During drying-wetting cycles the resultant shear modulus, water content and volume was measured at five discrete points. These measurements took place during the 1st (D/W1), 3rd (D/W3), 6th (D/W6) and 10th (D/W10) cycle. Four drying-wetting testing conditions were investigated, illustrated in Figure 6, including: FT full saturation to transition zone, CT compacted OMC to transition zone, FR full saturation to residual conditions and CR compacted OMC to residual conditions. Following compaction specimens were dried from the compacted water content at constant water contents levels to two drying boundaries including w_T=15% water content, selected within the linear section of transition zone, and w_R=1.5% water content chosen within proximity to residual conditions. This was followed wetting to two wetting boundaries including fully saturated conditions S_r=1.0 and Proctor compaction water content w_{OMC}=28%.

Drying boundaries allow for a direct comparison between the effect of transition zone and residual conditions. Drying within the transition zone is consistent with negative pore water pressure reported by Glendinning et al. (2014) for the Achilles test embankment which showed a range of between -300 and -600 kPa pore pressure at 1m depth during summer 2009 for the glacial till fill material compacted to National Highways specifications (National Highways, 2016). Wetting boundaries limited by the compacted moisture content (w_{OMC}=28%) permits the evaluation of contrasting fully saturated pathways on soil behaviour.

To achieve full saturation, specimens were submerged in demineralized water under vacuum pressure facilitating the removal of entrapped air. Results showed the adopted method consistently achieved the required maximum saturation. Specimens were encased in a latex membrane and ridged mould to preserve their initial diameter during swelling (latex membranes have a modulus in extension of 1050 kPa when 0.2mm thick) (Raghunandan et al., 2015). Specimen desaturation was conducted by air-drying at a constant 40℃ temperature to simulate loss of moisture through evaporation. The drying temperature was chosen to expedite drying, as it was expected to have little impact on the mechanical response of the soil. Furthermore, this temperature is commonly experienced by compacted soils in several countries. During testing water content controlled the degree of drying, determined by specimen weight, as the mass of solids remained constant. Partially saturated paths were wetted to the compacted water content by the addition of the required amount of water by weight. Specimens were encased in similar conditions to fully saturated specimens.

To ensure the even distribution of moisture throughout each wetting or drying stage specimens were left at constant temperature to equilibrate. To inform the time required, the distribution of water content was determined for fully saturated conditions (46.5% water content), 15% water content and 1.5% water content. These conditions were tested for equilibration times of 1hr, 12hrs and 24hrs. The results shown in Figure 7 demonstrate that initially after 1hour equilibration wetting and drying produced substantial variations in water content throughout the specimens both laterally and vertically. However, a further 24 hour equilibration period minimized moisture variation to <0.5%. Thus, 24 hours was adopted as a minimum equilibration period after alterations were made to a specimens water content, to ensure uniform hydraulic pathways were imposed.

3 RESULTS AND DISCUSSION

3.1 Shear Modulus Variation with Water Content

During drying and wetting to chosen constant water content levels, shear wave data was collected at discrete points. Figure 8 shows an example of the typical shear wave evolution for kaolin during the first drying-wetting cycle between the compacted water content and the transition zone (CT). It can be observed during initial drying from a water content of w_{OMC}= 28% to the driest point w_T= 15%, the shear wave arrival time decreases by 72 µs. However, upon wetting back to the compacted water content (w_{OMC}= 28%) the shear wave arrival time was delayed by 113 µs. This represents a 41 µs decrease in arrival time at the compacted water content on the wetting path as a result of hysteresis of capillary water (Dong and Lu, 2016). Notably this is contrary to suction controlled testing where arrival times on the drying path are slower when compared to wetting paths.

Figure 9 presents the shear wave velocity data for the first drying-wetting cycle (CT). Figure 9(a) confirms that when the data is plotted using gravimetric water content, the drying path exhibits greater shear wave velocity at the water content levels considered. However, when the data is again plotted using suction values (Figure 9(b)) the trend is inverted (i.e. higher shear wave velocity on the wetting path) as reported in previous studies (Khosravi and McCartney, 2012; Ngoc et al., 2019; Ng et al., 2009; Heitor et al., 2015a).

As expected, Figure 9 also shows that drying-wetting cycles controlled by gravimetric water content induce differences in suction values. This is associated with the soil pore structure, i.e. water re-enters the macropores first and is affected by contact angle and entrapped air (Hillel, 2003). The decreased suction on the wetting path in combination with the reduction of shear wave velocity, inverts the hysteresis cycle in the small strain stiffness -

suction space. This is further exemplified when the data is plotted in the gravimetric water content - suction space (Figure 9(c)). In this case the hysteresis loop again shows the equivalent behavior to Figure 9(a). The discrepancy in hysteresis loop configuration between water content and suction approaches is thus a consequence of the representation of data in the suction - small strain stiffness space, as the control of suction is generally requisite of the axis translation technique. The axis translation approach generally requires saturation to be reduced (coupled with water content) on the wetting path to reach a selected suction level. However, when this is presented in a water content – small strain stiffness space, the behavior is consistent with Figure 9(a). The distinction between the configurations of hysteresis loops is important when considering behaviour of material in practice. In this case, matric suction changes are commonly a consequence of changes in water content resulting from soil-atmosphere interactions including evaporation, evapotranspiration and infiltration. Furthermore, the consideration of water content has additional advantages in light of recent advancement in satellite imagery using L-band Synthetic Aperture Radar (Ahlmer et al., 2018) that enable the determination of water content non-destructively.

The evolution of the shear modulus during the selected hydraulic pathways at selected water content levels, illustrated in Figure 6, are presented in Figure 10. In total, 16 compacted kaolin specimens were monitored, and shear wave velocity and volumetric strain data for the four selected drying and wetting domains was evaluated. Measurements were made at the selected constant water content levels to allow for the evaluation of the evolution of soil behavior in the drying-wetting cycles. No measurements were made at full saturation because specimens were very soft. Thus, to minimise specimen disturbance measurements were conducted at the compacted water content (w_{OMC}=28%) which correlated to an increase in stiffness suitable for testing. Furthermore, its important to note that there were no visible macroscopic cracks during drying-wetting which impacted the integrity of the specimens. Results are presented against water content for drying-wetting cycles 1, 3, 6 and 10.

Figure 10 shows that shear modulus values measured for the different drying-wetting cycles are inversely correlated to water content, i.e. at low water contents a higher shear modulus is measured, whereas shear modulus decreases as the water content increases. This is not surprising as the matric suction levels in the specimens are quite different, with approximately 2,500 kPa increase in matric suction between w_{OMC}=28% and w_T=15% water contents on the first drying path (Figure 9(c)). Equally, the range of water content values during drying influences the small strain shear modulus for an increment of water content. For instance, during drying within the transition zone (FT and CT), an approximately linear increase in small strain shear modulus is reported for an increment of water content (Figure 10(a,c)). However, drying to the residual range (FR and CR) yields a comparative reduction in the rate of small strain shear modulus increase (Figure 10(b,d)).

Within the transition zone (FT and CT) a pendular state develops and the meniscus effect dominates the increase in normal force between particles (Dong et al., 2017). Figure 3 shows that in this range the increase in suction is approximately linear when compared to water content. Thus, the increase in stiffness and small strain shear modulus of the kaolin essentially reflects the SWRC. However, at the lower water content range within residual conditions (FR and CR) the formation of the partial pendular state is likely to reduce the meniscus radius and Equivalent Effective Stress (EES) (Cho and Santamarina, 2001). Furthermore, Van der Waals attractions and electric double layer repulsions dominate in this state rather than the meniscus effect; although both exist simultaneously and develop gradually as water content changes (Lu, 2016). These forces are proportional to particle size and pore size and influence clays sized particles to greater extent compared to silts (Ngoc et al., 2019). The compacted kaolin shows a reduced rate of small strain shear modulus change within this range (i.e between w_T= 15% and w_R= 1.5%) on its first drying-wetting cycle (exemplified in Figure 10(b,d)). This model of small strain shear modulus evolution holds true during subsequent drying and wetting cycles when changes in void ratio are also considered (FR and PR at w_R= 1.5% water content).

The evolution of small strain shear modulus data for FT/FR/CT/CR pathways against the number of drying-wetting cycles is shown in Figure 11. The data shows that within the first 6 drying-wetting cycles a decrease in hysteresis loop amplitude between drying and wetting paths for the CT and CR conditions is present (Figure 11(c,d)). This is corroborated by measurement of void ratio for these pathways which show smaller volumetric changes. Similar observations have also been reported by Farulla et al. (2010) and Liu et al. (2020) for drying-wetting paths, e.g. reduction in the difference of matric suction between hysteresis loops after application of hydraulic cycles. This was also exemplified by Stirling et al. (2020) for results of continuous suction and water content on statically compacted glacial till during three drying and wetting cycles. It was shown that repeated drying between saturated conditions and 500 kPa suction resulted in a 50 kPa decrease on the drying path at constant 22% water content.

Curiously, both hydraulic pathways FT and FR generally exhibit increases in small strain shear modulus during the drying path for the first 6 cycles at their compacted water content (wOMC= 28%), but approximately constant shear modulus during wetting (Figure 11(a,b)). These changes are not surprising and can be related to the associated changes in microstructure. Hydraulic path FR also shows a significant increase in the small strain shear modulus within the residual state at w_R= 1.5% water content (Figure 11(b)). These increases also suggest a change within the micro pore structure as both suction and other inter particle forces within this state are dependent on pore diameters.

3.2 Void Ratio Variation with Drying-Wetting

Changes in void ratio directly affect the properties of the soil such as porosity, density and degree of saturation, which are critical to compacted soils performance. In this study volume changes were measured using Vernier calipers for eight discrete points to allow for calculation of volume using average dimensions to ensure accuracy (Head, 1996). Volume change of the specimens is presented using the water ratio, defined as the ratio of the volume of water to the volume of solids, against void ratio. Both variables are normalized against the volume of solids thus indicative of the volume change of the specimen with respect to the volume of water (i.e. equal void and water ratios indicate full saturation). The variation in computed void ratio (e) and water ratio (e_w) for all specimens and their associated hydraulic pathways are shown in Figure 12.

Data reveals that all kaolin specimens exhibit hysteric behavior between drying and wetting paths, where at selected water content levels during a wetting pathway, swelling is greater than on the drying path. This coincides with the reduction in suction during wetting due to SWRC hysteresis. When comparing these changes in void ratio with the corresponding results for shear modulus, common trends are visible. Most noticeably, small strain shear modulus is inversely proportional to void ratio data, where increases in void ratio yields a decrease in shear modulus during drying-wetting.

Its also evident that the amplitude of drying and wetting paths had a significant impact on changes in volume during the 10 drying-wetting cycles. For instance, specimens dried to the residual conditions (CR) showed a larger increase in void ratio from 0.930 to 0.971 at the compacted water content (w_{OMC}= 28%) after the first drying and wetting cycle (Figure 12(d)). However, specimens dried to the transition zone (CT) showed a smaller void ratio increase after the first cycle from 0.926 to 0.953 (w_{OMC}= 28%) (Figure 12(c)).

These increases can be attributed to a decrease in the Equivalent Effective Stress (EES) during drying (Vesga, 2008). The EES accounts for capillary forces; as well as Van der Waal attraction, double layer repulsion and Coulomb electrostatic forces (Cho and Santamarina, 2001). Reduction in water content produces a complete pendular state where the water phase in no longer continuous and all capillary bridges between particles are formed. For the compacted kaolin specimens shown in Figure 12 this state is likely present for drying to a degree less than w_T= 15% (i.e. Figure 12(b,d)) as prior to this point reduction in water content produces expected changes in volume (i.e. Figure 12(a,c)).

With further reduction in water content the partial pendular state develops (Suits et al., 2009). In this state the capillary contacts between particles break producing a reduction in the

EES due to loss of surface tension. In this study the breaking of capillary contacts is observed by the increase in volume of the compacted kaolin. For example, the first drying-wetting cycle of the FR pathway between w_T= 15% water content and w_R= 1.5 % water content showed an increases in void ratio of 0.925 to 0.962 (Figure 12 (b)).

Interestingly, as wetting and drying continues theses changes in structure are maintained, particularly when full saturation is not reached, and continue to allow for an increase in void ratio. This is shown in Figure 12(d) (CR) where void ratio increases from 0.961(D/W1) to 1.01 (D/W10) at w_R= 1.5 % water content after 10 drying-wetting cycles. Furthermore, when compared with the equivalent saturated pathway (FR) in Figure 12(b) its clear that saturation has an effect on the kaolin producing a decrease in void ratio after 10 drying-wetting cycles at the same water content level despite the initial large void ratio increase.

These changes in volume during drying-wetting indicate changes in the pore structure of the specimens (Thom et al., 2007; Nowamooz et al., 2016) For instance, this can observed when comparing specimens both dried to residual conditions (FR) and dried to the transition zone (FT). During the first wetting cycle of FT, the void ratio increases from 0.913 to 0.949 when wetting between w_T=15% and w_{OMC}=28% (Figure 12(a)). Whereas, the first wetting cycle of FR, the void ratio only increases from 0.961 to 0.971 between w_R=1.5% and w_{OMC}=28% despite the larger change in water content (Figure 12(b)). This is likely due to difference in packing of the aggregates resulting from the prior volume changes during drying.

3.3 The Effects of Hydraulic Pathway on Small Strain Shear Modulus

Figure 13 shows the normalized change in shear modulus from compacted conditions at selected water content levels for both drying and wetting paths. A clear distinction is observed between the fully saturated boundary (FT/FR) and compacted water content wetting boundary (w_{OMC} = 28%) (CT/CR). In general, specimens brought to full saturation during drying-wetting (FT/FR) exhibit increases in shear modulus for increasing drying wetting cycles (Figure 13(a-g)). In contrast, specimens wetted to the compacted water content (CT/CR) during drying-wetting experienced a decrease in shear modulus (Figure 13(a-g)). It should be noted that this trend is reflected on both drying and wetting pathways irrespectively of the water content level represented. Notably, the data also shows that drying to residual conditions produces a decrease (Figure 13(a,b,e,f and g) FR conditions) or increase (Figure 13 (a,b,e,f and g) CR conditions) in the rate of shear modulus change at all water contents, of which w_{OMC}= 28% (Figure 13(a)) shows the largest variation. For instance, the drying CR pathway at w_{OMC}= 28% (Figure 13(b)) resulted in a 35% reduction in shear modulus compared to compacted conditions after 10 drying-wetting cycles ($G_{max}/G_{max\text{-}initial}$ =0.65), whereas, comparable CT conditions yielded a smaller 21% reduction ($G_{max}/G_{max\text{-}initial}$ =0.79). Conversely, the FT pathway at w_{OMC}= 28% (Figure 13(a)) showed a 29% increase in shear modulus after 10 drying-wetting cycles ($G_{max}/G_{max\text{-}initial}$ = 1.29), while the drying FR pathway produced a smaller 8% increase ($G_{max}/G_{max\text{-}initial}$ = 1.08).

These results indicate that the wetting boundary has the greatest influence on the behavior of the specimens rather than the degree of drying. In this study, only fully saturated and compaction water content boundaries were considered and a reversal in the shear modulus behavior was observed. In addition, this reversal behavior seems to be far more significant at the wetter end (w_{OMC}= 28%) (Figure 13(a,b)). The recorded trends further suggest that drying boundaries influence the magnitude of the change observed, e.g. similar variations were observed between the increase in shear modulus for FT and FR and the decrease in shear modulus for CT and CR. This is not surprising and can be attributed to the changes in microstructure specimens exhibit at the drying boundaries.

Figure 14 further explores this by presenting recorded volumetric strain data at the boundaries of drying-wetting cycles for all pathways. The volumetric strain is determined considering the ratio between the variation volume and the initial compacted volume, shown as a percentage. It shows that both fully saturated pathways exhibit large swelling strains when brought to full saturation (Figure 14(a) FT pathway produced ε_{vs} of 13% after first full saturation). While specimens brought to compacted water content experienced smaller degrees of volumetric strain variation (Figure 14(c) CT pathway produced ε_{vs} of 1% after first wetting to 28% water content). Furthermore, fully saturated pathways (Figure 14(a,b)) are dominated by an irreversible shrinkage strain component with asymptotic behaviour. In contrast, specimens brought to compacted water content (Figure 14(c,d)) exhibit a similar asymptotic irreversible swelling strain. The reversal observed for shear modulus measurements strongly correlates with this behaviour.

Interestingly, Figure 14(b) pathway FR, also shows evidence of irreversible swelling at the drying boundary (w_R= 1.5% water content) within the first three cycles, while also presenting subsequent irreversible shrinkage. This contrasts with the equivalent CR pathway (Figure 14(d)) which shows continuous irreversible swelling at this drying boundary. This therefore confirms the presence of interactions between both wetting and drying boundaries. Wang and Wei (2015) suggests that the deformation of compacted soils results from both the rearrangement of the skeleton of the aggregates and the deformation of the aggregates. Irreversible swelling/shrinkage represents rearrangement of the pore structure in this respect. While attainment of equilibrium represents the reversible deformation of aggregates during changes in water content. These accumulated irreversible changes in volumetric strain have been characterized, for a small number of cycles only, by several researchers including Koliji et al. (2010); Nowamooz et al. (2016); Farulla et al. (2010); Ma, R. et al. (2015); Sun and Cui (2018) corresponding with significant changes in the pore structure of the soil. These findings corroborate the empirically supported presupposition of irreversible structural changes and demonstrate for the first time that the associated observed changes in small strain stiffness are highly dependent on hydraulic loading conditions.

4 Engineering Applications

Figure 15 shows the relationship between void ratio and shear modulus during 10 drying wetting cycles grouped by constant water content. The most striking observation is that the small strain shear modulus grouped by different water content levels can be fitted with a linear relationship. Figure 15 also presents the pathways for initial drying and wetting data for FT/CT and FR/CR. It shows that data for all chosen boundaries lie on the same linear trends in spite of difference in outcome. The trends are thus independent of the number of cycles and drying and wetting boundaries.

Furthermore, the observed trend is approximately the same at all recorded water contents, which is notable due to the large difference in water content . However, as measurements were made at constant water content, changes in void ratio result in equal changes in saturation i.e. an increase in void ratio produces an equivalent decrease in saturation. These changes result in nonlinear changes in suction according to the SWRC in the S_r-s-e space. However, it can be ascertained in Figure 15 that differences in void ratio and saturation at constant water content levels are relatively small over the 10 drying-wetting cycles. For instance, at constant w_{OMC}= 28% water content the minimum void ratio equals 0.926 resulting in a small strain shear modulus 114 MPa and saturation of 78.7%. While the corresponding maximum value of void ratio equals 1.025 for a small strain shear modulus of 71 MPa and saturation of 74.9%. Thus, changes in suction due to the difference in saturation are likely to be relatively small, which may explain why the trend appears linear across the range or recorded void ratios.

The constant water content conditions employed in this study therefore show that unconfined compacted kaolin clay presents an approximate linear change in small strain shear modulus for an increment of void ratio change due to drying and wetting. The existence of such relationship is very encouraging as there is a great uncertainty at the moment in relation to the role of different wetting and drying boundaries and their impact on performance of existing transport infrastructure assets. In practice, this understanding is also beneficial when estimating the range of variation of performance and volume changes likely to be expected for intermediate plasticity soil with similar properties to that of kaolin. This is particularly important for the consideration of the performance of high-speed rail which is sensitive to rail deflections dependent on the critical speed of the subgrade (Shih et al., 2017). Dynamic loading and resultant ground borne vibration emitted at the critical speed (determined by the speed of Rayleigh waves) results in increased strains according to the non-linearity small strain conditions (Costa et al., 2020). The results demonstrate significant variations in stiffness of compacted materials due to difference in the oscillations of water content over relatively small changes in volume. These results highlight for the first time how the properties of compacted subgrade change during drying and wetting, and hence, a possible impact of climate change on earth structures for transport infrastructure.

5 CONCLUSIONS

From a series for non-destructive tests carried out on compacted kaolin subjected to 10 dying and wetting cycles, a number of conclusions can be drawn:

When small strain data is presented using water content the shear wave velocity on drying path is greater than the wetting path. However, when the same data is presented against suction this trend is inverted, which corresponds with data collected at selected suction levels using axis translation technique.

A nonlinear increase in small strain shear modulus due to changes in water content was observed. Where, at lower water contents (1.5% water content) the rate of increase in shear modulus reduces. Furthermore, drying-wetting cycles produced a decrease in hysteresis loop amplitude between drying and wetting paths for all drying-wetting conditions.

Similarly, drying to lower water contents (1.5% water content) results in increase in void ratio. Evidence suggests that this occurs due to the development of the partial pendular state where capillary contacts break and the Equivalent Effective Stress (EES) decreases. The measured changes in small strain shear modulus are consistent with these changes in void ratio.

The wetting boundary was found to have the greatest impact on the compacted soil behavior after the application of several drying-wetting cycles. A reversal of both small strain shear modulus and volume change was observed and this was associated with the drying-wetting boundaries considered. For instance, fully saturated boundary conditions (FT/FR) resulted in the increase in small strain shear modulus and comparative reduction in void ratio. While the compacted water content wetting (CT/CR) boundary conditions resulted in an asymptotic decrease in small strain shear modulus and increase in void ratio. Although drying boundaries did not have as large impact on behavior, the residual conditions boundary (FR/CR) decreased the performance of the compacted kaolin when subjected to drying-wetting cycles.

A clear linear trend is observed between void ratio and small strain shear modulus at different water content levels. This trend is approximately comparable for all measured water contents and is relatively independent of the number of drying-wetting cycles and the selected boundaries. This indicates that predictions of small strain stiffness is well correlated to volume changes and water content.

Data Access statement: All data underlying the results are available as part of the article and no additional source data are required

Authors contribution: The contribution from the different authors can be summarised as follows. Conceptualization, all authors; writing—original draft preparation and laboratory testing, C.W.; writing—review and editing, all authors, project supervision - AH. All authors have read and agreed to this version of the manuscript.

Acknowledgements: The author gratefully acknowledges the support provided by the School of Civil Engineering, University of Leeds and financial support provided by EPSRC Doctoral Training Program, (grant number EP/T517860/1). The laboratory assistance provided by Andrew Birch from the University of Leeds is gratefully appreciated.

References

Ahlmer, A.-K., Cavalli, M., Hansson, K., Koutsouris, A.J., Crema, S. and Kalantari, Z. 2018. Soil moisture remote-sensing applications for identification of flood-prone areas along transport infrastructure. *Environmental Earth Sciences.* **77**(14), p533.

Arulnathan, R., Boulanger, R.W. and Riemer, M. 1998. Analysis of Bender Element Tests. *Geotechnical Testing Journal.* **21**, pp.120-131.

ASTM D5298-10. 2010. *Standard test method for measurement of soil potential (suction) using filter paper* West Conshohocken, PA, USA: ASTM International

Azizi, A., Musso, G. and Jommi, C. 2019. Effects of repeated hydraulic loads on microstructure and hydraulic behaviour of a compacted clayey silt. *Canadian Geotechnical Journal.* **57**(1), pp.100-114.

Azizi, A., Musso, G., Jommi, C. and Cosentini, R. 2018. Evolving fabric and its impact on the shearing behaviour of a compacted clayey silt exposed to drying-wetting cycles. *7th International Conference on Unsaturated Soils.*

British Standards Institution. 2022. BS 1377-2:2022. *Methods of test for soils for civil engineering purposes. Classification tests and determination of geotechnical properties.* London: BSI.

Cheng, Z. and Leong, E.C. 2014. A Hybrid Bender Element–Ultrasonic System for Measurement of Wave Velocity in Soils. *Geotechnical Testing Journal.* **37**, p20120158.

Cho, G.C. and Santamarina, J.C. 2001. Unsaturated Particulate Materials—Particle-Level Studies. *Journal of Geotechnical and Geoenvironmental Engineering.* **127**(1), pp.84-96.

Clarke, B.G. 2018. The engineering properties of glacial tills. *Geotechnical Research.* **5**(4), pp.262-277.

Clarke, D. and Smethurst, J.A. 2010. Effects of climate change on cycles of wetting and drying in engineered clay slopes in England. *Quarterly Journal of Engineering Geology and Hydrogeology.* **43**(4), pp.473-486.

Costa, P.A., Soares, P., Colaço, A., Lopes, P. and Connolly, D. 2020. Railway critical speed assessment: A simple experimental-analytical approach. *Soil Dynamics and Earthquake Engineering.* **134**, p106156.

Da Fonseca, A., Ferreira, C. and Fahey, M. 2009. A Framework Interpreting Bender Element Tests, Combining Time-Domain and Frequency-Domain Methods. *Geotechnical Testing Journal - GEOTECH TESTING J.* **32**.

Dong, Y. and Lu, N. 2016. Dependencies of Shear Wave Velocity and Shear Modulus of Soil on Saturation. *Journal of Engineering Mechanics.* **142**(11), p04016083.

Dong, Y., Lu, N. and McCartney, J. 2017. Scaling Shear Modulus from Small to Finite Strain for Unsaturated Soils. *Journal of Geotechnical and Geoenvironmental Engineering.* **144**.

Farulla, C.A., Ferrari, A. and Romero, E. 2010. Volume change behaviour of a compacted scaly clay during cyclic suction changes. *Canadian Geotechnical Journal.* **47**(6), pp.688-703.

Genuchten, V. 1980. A closed-form Eq. for predicting the hydraulic conductivity of unsaturated soils. *Soil Science Journal.* **44**, pp.892-898.

Glendinning, S., Helm, P., Rouainia, M., Stirling, R., Asquith, J., Hughes, P., Toll, D., Clarke, D., Powrie, W., Smethurst, H., Hughes, D., Kelly, R. and Karim, M. 2015. Research-informed design, management and maintenance of infrastructure slopes: development of a multi-scalar approach. *IOP Conference Series: Earth and Environmental Science.* **26**, pp.207-215.

Glendinning, S., Hughes, P., Helm, P., Chambers, J., Mendes, J., Gunn, D., Wilkinson, P. and Uhlemann, S. 2014. Construction, management and maintenance of embankments used for road and rail infrastructure: implications of weather induced pore water pressures. *Acta Geotechnica.* **9**(5), pp.799-816.

González, N.A. and Colmenares, J.E. 2006. Influence of Matric Suction on the Volume Change Behaviour of a Compacted Clayey Soil. *Unsaturated Soils 2006.* pp.825-836.

Head, K.H. 1996. *Manual of soil laboratory testing.* Second edition. ed. Chichester: Wiley.

Heitor, A. 2013. *Assessment of post-compaction characteristics of an unsaturated silty sand*. Doctor of Philosophy thesis, University of Wollongong.

Heitor, A., Indraratna, B. and Rujikiatkamjorn, C. 2015a. Effect of suction history on the small strain response of a dynamically compacted soil. *12th Australia - New Zealand Conference on Geomechanics (Wellington, 2015).* **50**, pp.61-68.

Heitor, A., Indraratna, B. and Rujikiatkamjorn, C. 2015b. The role of compaction energy on the small strain properties of a compacted silty sand subjected to drying–wetting cycles. *Géotechnique.* **65**(9), pp.717-727.

Khosravi, A. and McCartney, J.S. 2012. Impact of Hydraulic Hysteresis on the Small-Strain Shear Modulus of Low Plasticity Soils. *Journal of Geotechnical and Geoenvironmental Engineering.* **138**(11), pp.1326-1333.

Koliji, A., Vulliet, L. and Laloui, L. 2010. Structural characterization of unsaturated aggregated soil. *Canadian Geotechnical Journal.* **47**(3), pp.297-311.

Krautkrämer, J., Krautkrämer, H. and Grabendörfer, W. 1990. *Ultrasonic testing of materials.* Fourth fully revised edition. ed. Berlin ;: Springer.

Leong, E., Sir Hoon, Y. and Rahardjo, H. 2011. Measurement of wave velocities and attenuation using an ultrasonic test system. *Canadian Geotechnical Journal.* **41**, pp.844-860.

Leong, E.C. and Rahardjo, H. 2002. Factors Affecting the Filter Paper Method for Total and Matric Suction Measurements. *Geotechnical Testing Journal - GEOTECH TESTING J.* **25**.

Liu, G., Toll, D., Kong, L.-W. and Asquith, J. 2020. Matric Suction and Volume Characteristics of Compacted Clay Soil under Drying and Wetting Cycles. *Geotechnical Testing Journal.* **43**, p20170310.

Lowe, J., Bernie, D., Bett, P., Bricheno, L., Brown, S., Calvert, D., Clark, R., Karen, Eagle, Edwards, T., Fosser, G., Maisey, P., McInnes, R., Mcsweeney, C., Yamazaki, K. and Belcher, S. 2019. *UKCP 18 Science Overview Report November 2018 (Updated March 2019).* [Online]. [Accessed 11/05/2021]. Available from: https://www.metoffice.gov.uk/pub/data/weather/uk/ukcp18/science-reports/UKCP18-Overview-report.pdf

Lu, N. 2016. Generalized Soil Water Retention Equation for Adsorption and Capillarity. *Journal of Geotechnical and Geoenvironmental Engineering.* **142**(10), p04016051.

Ma, C., Li, J., Jiao, F., Liu, Y., Feng, H., Wang, K., Jiang, H., Jiang, C., Li, Y. and Geng, X. 2023. Physical and Mechanical Behaviors of Compacted Soils under Hydraulic Loading of Wetting–Drying Cycles. *Processes.* **11**(4), p1084.

Ma, R., Cai, C., Li, Z., Wang, J., Xiao, T., Peng, G. and Yang, W. 2015. Evaluation of soil aggregate microstructure and stability under wetting and drying cycles in two Ultisols using synchrotron-based X-ray micro-computed tomography. *Soil and Tillage Research.* **149**, pp.1-11.

Nakagawa, K., Soga, K. and Mitchell, J.K. 1996. Pulse Transmission System for Measuring Wave Propagation in Soils. *Journal of Geotechnical Engineering.* **122**(4), pp.302-308.

National Highways. 2016. *Manual of Contract Document for Highway Works, Volume 1 - Specification for Highway Works, Series 600 - Earthworks. National Highways.* [Online]. [Accessed 25 August 2022]. Available from: www.standardsforhighways.co.uk

Ng, C.W.W., Xu, J.X. and Y.Yung, S. 2009. Effects of wetting–drying and stress ratio on anisotropic stiffness of an unsaturated soil at very small strains. *Canadian Geotechnical Journal.* **46**(9), pp.1062-1076.

Ngoc, T.P. 2020. *Experimental Study on the Small Strain Shear Modulus of Unsaturated Soils*. PhD thesis, University of Technology Sydney.

Ngoc, T.P., Fatahi, B. and Khabbaz, H. 2019. Impacts of Drying-Wetting and Loading-Unloading Cycles on Small Strain Shear Modulus of Unsaturated Soils. *International Journal of Geomechanics.* **19**(8), p04019090.

Nowamooz, H., Jahangir, E., Masrouri, F. and Tisot, J.-P. 2016. Effective stress in swelling soils during wetting drying cycles. *Engineering Geology.* **210**, pp.33-44.

Raghunandan, M.E., Sharma, J.S. and Pradhan, B. 2015. A review on the effect of rubber membrane in triaxial tests. *Arabian Journal of Geosciences.* **8**(5), pp.3195-3206.

Reddy, B. and Jagadish, K. 1993. The static Compaction of Soils. *Geotechnique.* **43**, pp.337-341.

Reeves, G.M., Sims, I. and Cripps, J. 2006. Clay materials used in construction. *Geological Society Engineering Geology Special Publication.* **21**, pp.1-447.

Santamarina, J.C. 2003. Soil Behavior at the Microscale: Particle Forces. *Soil Behavior and Soft Ground Construction.* pp.25-56.

Shih, J.Y., Thompson, D.J. and Zervos, A. 2017. The influence of soil nonlinear properties on the track/ground vibration induced by trains running on soft ground. *Transportation Geotechnics.* **11**, pp.1-16.

Stirling, R.A., Toll, D.G., Glendinning, S., Helm, P.R., Yildiz, A., Hughes, P.N. and Asquith, J.D. 2020. Weather-driven deterioration processes affecting the performance of embankment slopes. *Géotechnique.* **71**(9), pp.1-13.

Suits, L., Sheahan, T. and Vesga, L. 2009. Direct Tensile-Shear Test (DTS) on Unsaturated Kaolinite Clay. *Geotechnical Testing Journal - GEOTECH TESTING J.* **32**.

Sun, W.-J. and Cui, Y.-J. 2018. Investigating the microstructure changes for silty soil during drying. *Géotechnique.* **68**(4), pp.370-373.

Tang, A.M., Vu, N. and Cui, Y. 2011. Effects of the maximum soil aggregates size and cyclic wetting–drying on the stiffness of a lime-treated clayey soil. In: *Partial Saturation in Compacted Soils*. Géotechnique, pp.35-43.

Tarantino, A. 2009. A water retention model for deformable soils. *Géotechnique.* **59**(9), pp.751-762.

Tarantino, A. and Col, E.D. 2008. Compaction behaviour of clay. *Geotechnique.* **58**(3), pp.199-213.

Tarantino, A. and Tombolato, S. 2005. Coupling of hydraulic and mechanical behavior in unsaturated compacted clay. *Geotechnique.* **55**(4), pp.307-317.

Thom, R., Sivakumar, R., Sivakumar, V., Murray, E.J. and Mackinnon, P. 2007. Pore size distribution of unsaturated compacted kaolin: the initial states and final states following saturation. *Géotechnique.* **57**(5), pp.469-474.

Vesga, L.F. 2008. Equivalent Effective Stress and Compressibility of Unsaturated Kaolinite Clay Subjected to Drying. *Journal of Geotechnical and Geoenvironmental Engineering.* **134**(3), pp.366-378.

Walker, C., Heitor, A. and Clarke, B. 2022. Influence of Weather-Driven Processes on the Performance of UK Transport Infrastructure with Reference to Historic Geostructures. *Applied Sciences.* **12**(15), p7461.

Wang, G. and Wei, X. 2015. Modeling swelling–shrinkage behavior of compacted expansive soils during wetting–drying cycles. *Canadian Geotechnical Journal.* **52**(6), pp.783-794.

Whalley, W.R., Jenkins, M. and Attenborough, K. 2012. The velocity of shear waves in unsaturated soil. *Soil and Tillage Research.* **125**, pp.30-37.

Ying, Z., Cui, Y.-J., Benahmed, N. and Duc, M. 2021. Changes of small strain shear modulus and microstructure for a lime-treated silt subjected to wetting-drying cycles. *Engineering Geology.* **293**, p106334.

Table 1. Summary of the index properties of the kaolin and target compaction conditions.

Geotechnical Properties	Value
Liquid Limit, LL (%)	56
Plastic Limit, PL (%)	33
Plastic Index, PI (%)	23
Specific gravity, G_s	2.61
Clay fraction (d< 2 µm) (%)	38
Maximum Proctor unit weight (kN/m³)	14.1
Optimum Water Content (OMC) (%)	28
Target Compaction Conditions	
Unit weight (kN/m³)*	13.2
Compaction water content (%)	28

**Unit weight achieved at static 1400 kPa stress*

Table 2. Ultrasonic variation in L_{pp}/λ during drying-wetting of compacted kaolin specimens.

Drying path		
Water Content (%)	**L_{pp}/λ - 24 kHz**	**L_{pp}/λ - 250 kHz**
28	7.0	72.7
21.5	5.7	59.5
15	5.0	51.7
1.5	4.5	47.1
Wetting path		
Water Content (%)	**L_{pp}/λ - 24 kHz**	**L_{pp}/λ - 250 kHz**
15	5.4	56.3
21.5	6.0	62.2
28	7.5	78.6

Table 3. Calculation of ultrasonic energy transmitted and reflected between transducer and statically compacted kaolin

Transmission/Reflection	
S Wave Reflection (%)	81.3
P Wave Reflection (%)	86.1
S Wave Energy Transmitted (%)	18.7
P Wave Energy Transmitted (%)	13.9

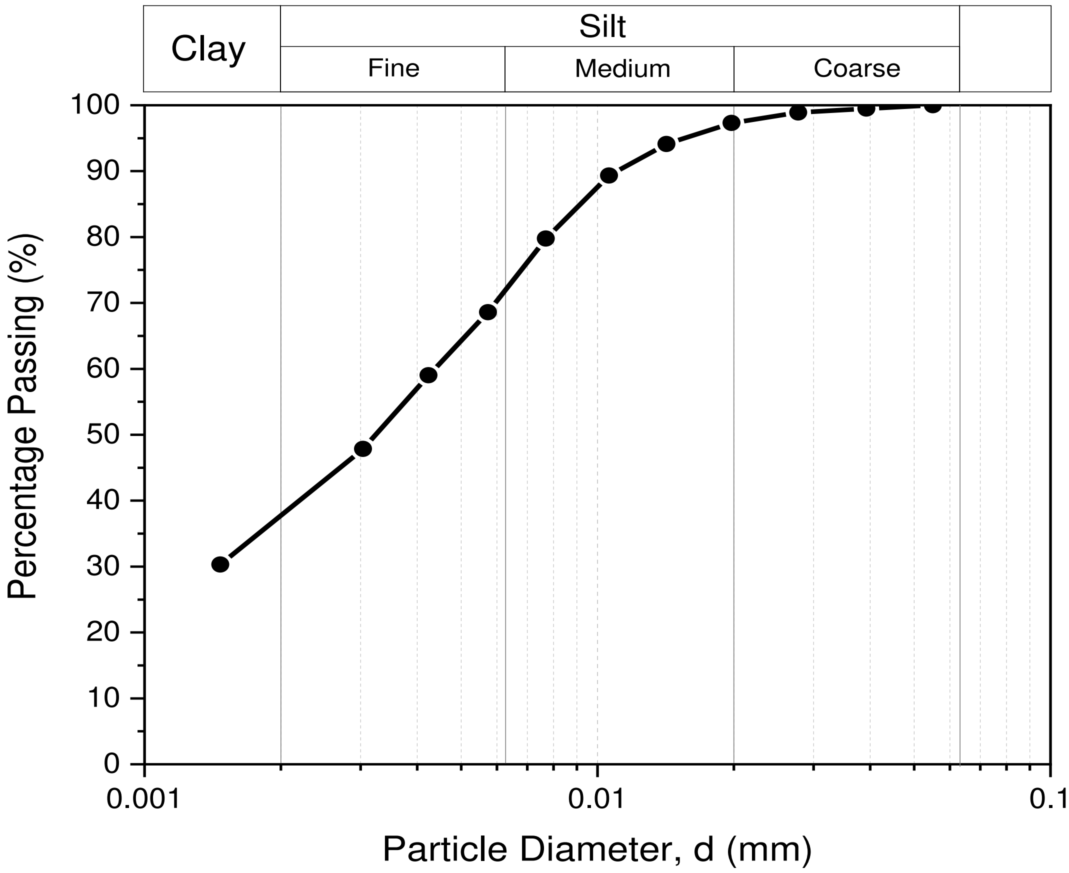

Figure 1. Particle size distribution of kaolin used in this study.

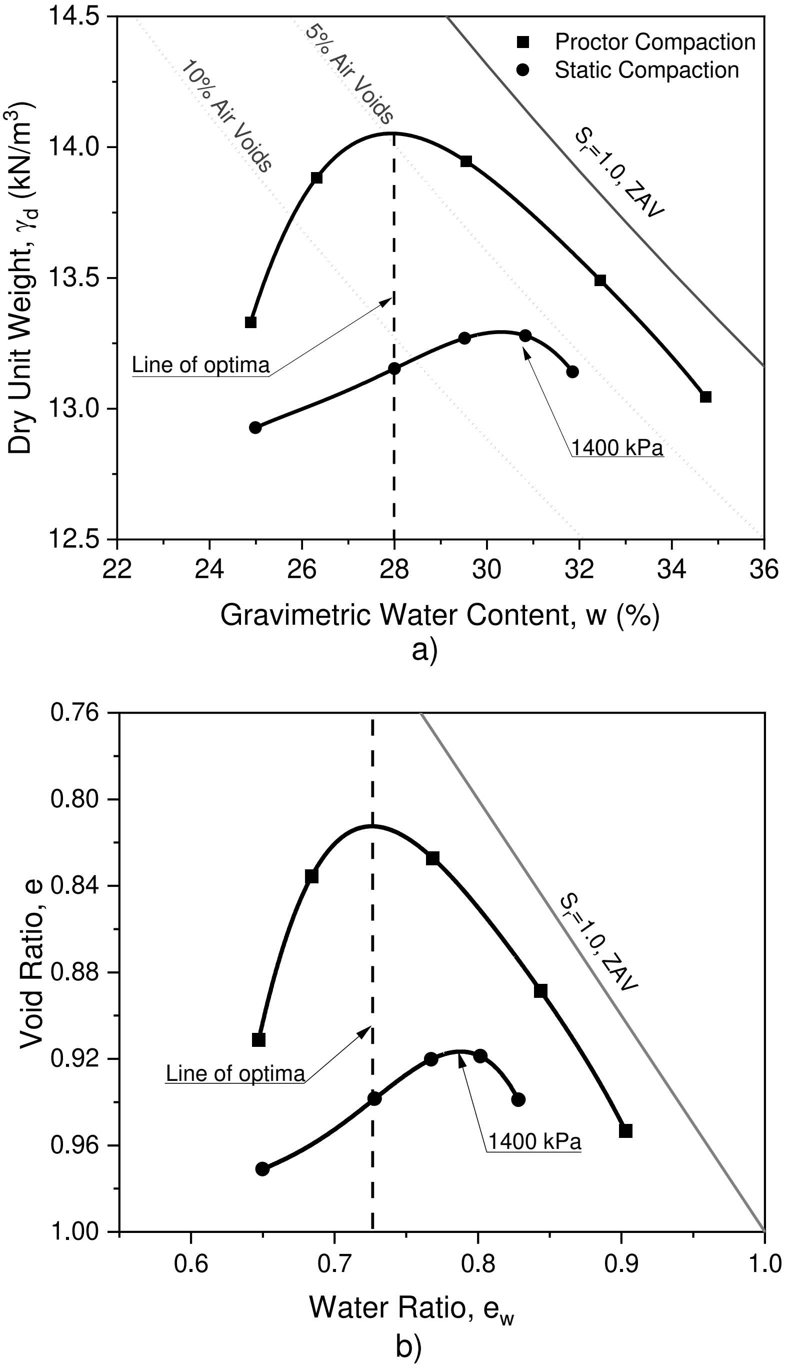

Figure 2. Compaction behaviour of kaolin: comparison between standard Proctor method (dynamic) and static compaction for both a) dry unit weight and water content and b) void ratio and water ratio (ZAV – zero air void line).

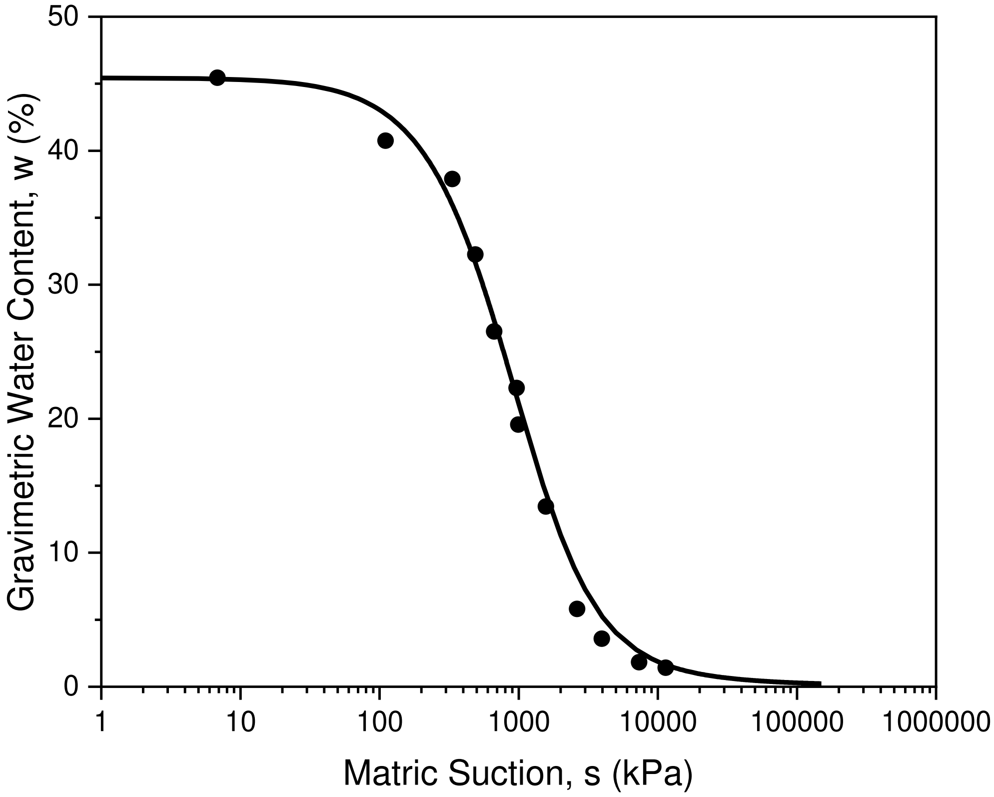

Figure 3. The Soil Water Retention Curve for kaolin statically compacted at 1400 kPa.

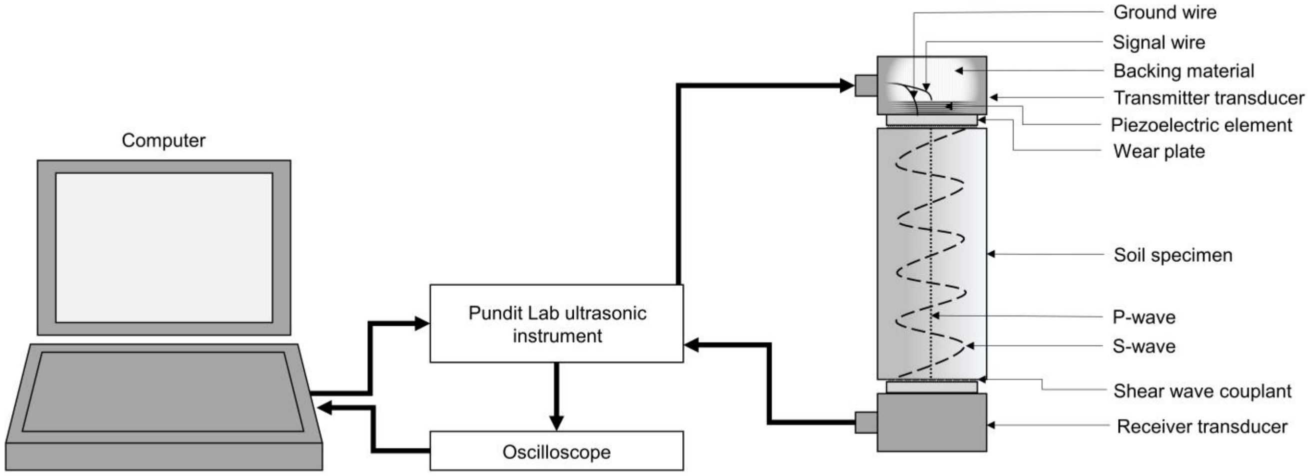

Figure 4. The experimental setup of ultrasonic test system.

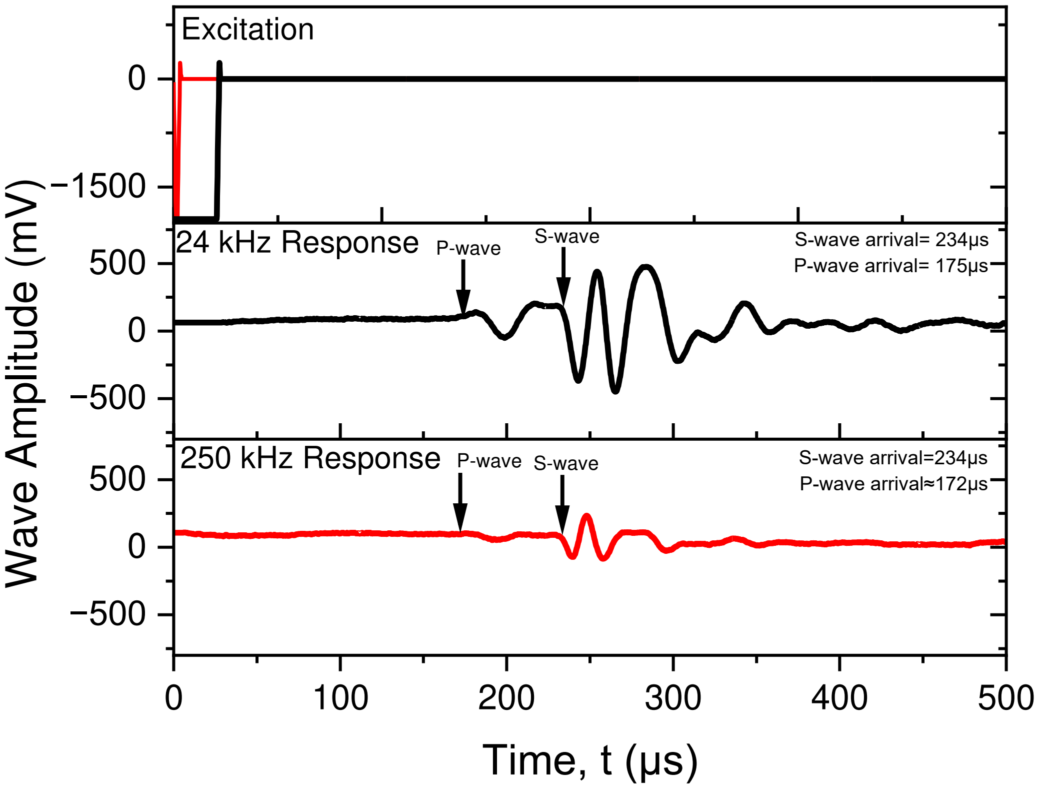

Figure 5. Typical shear wave time domain waveforms for compacted kaolin (prepared at optimum water content and statically compacted at 1400 kPa) at frequencies 24 kHz and 250 kHz, arrows identify the arrival of the faster compressional wave component and slower shear wave component.

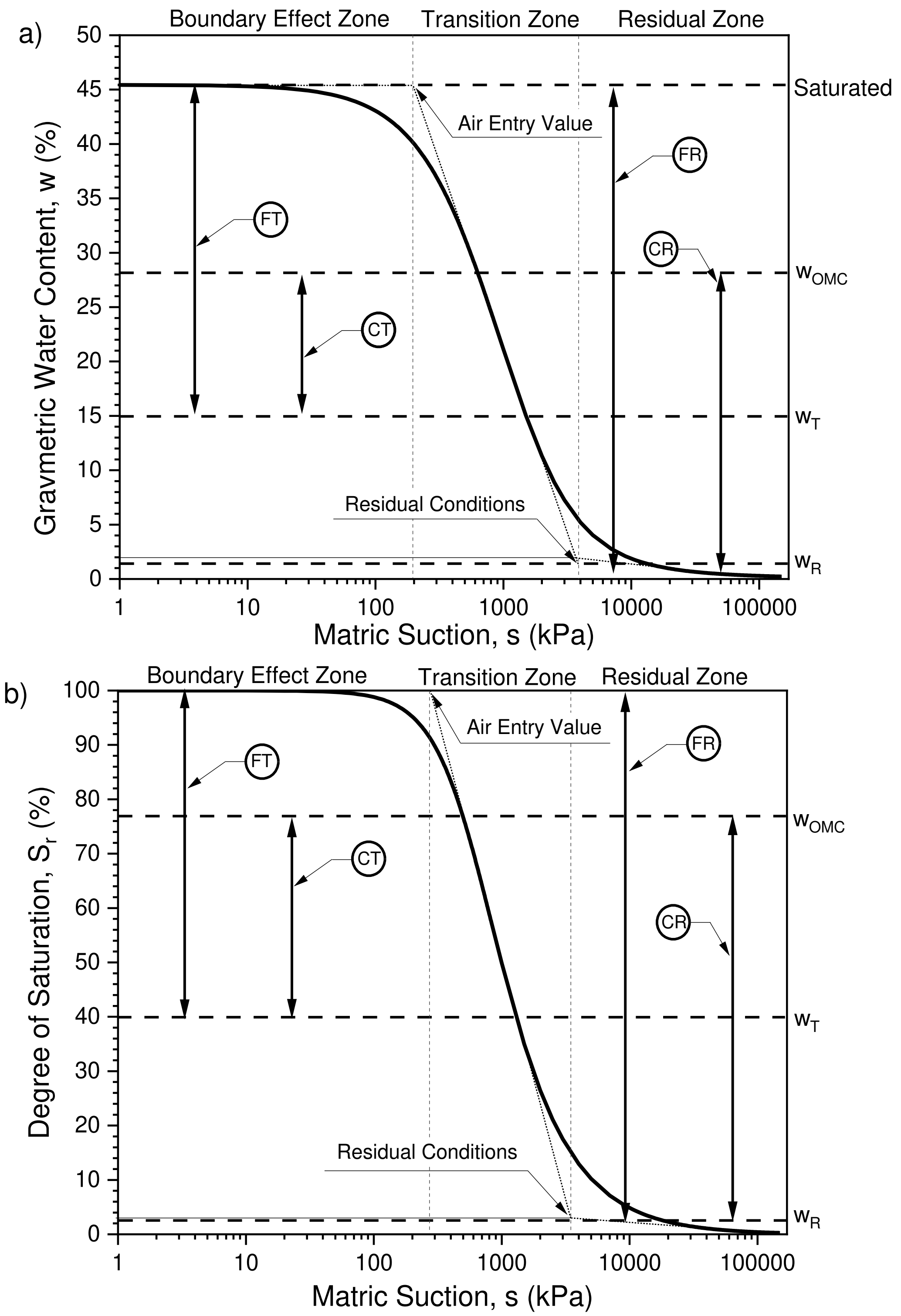

Figure 6. Extents of hydraulic paths expressed on the SWRC for: FT full saturation to transition zone, CT compacted OMC to transition zone, FR full saturation to residual conditions, CR compacted OMC to residual conditions, with reference to both a) water content and b) saturation.

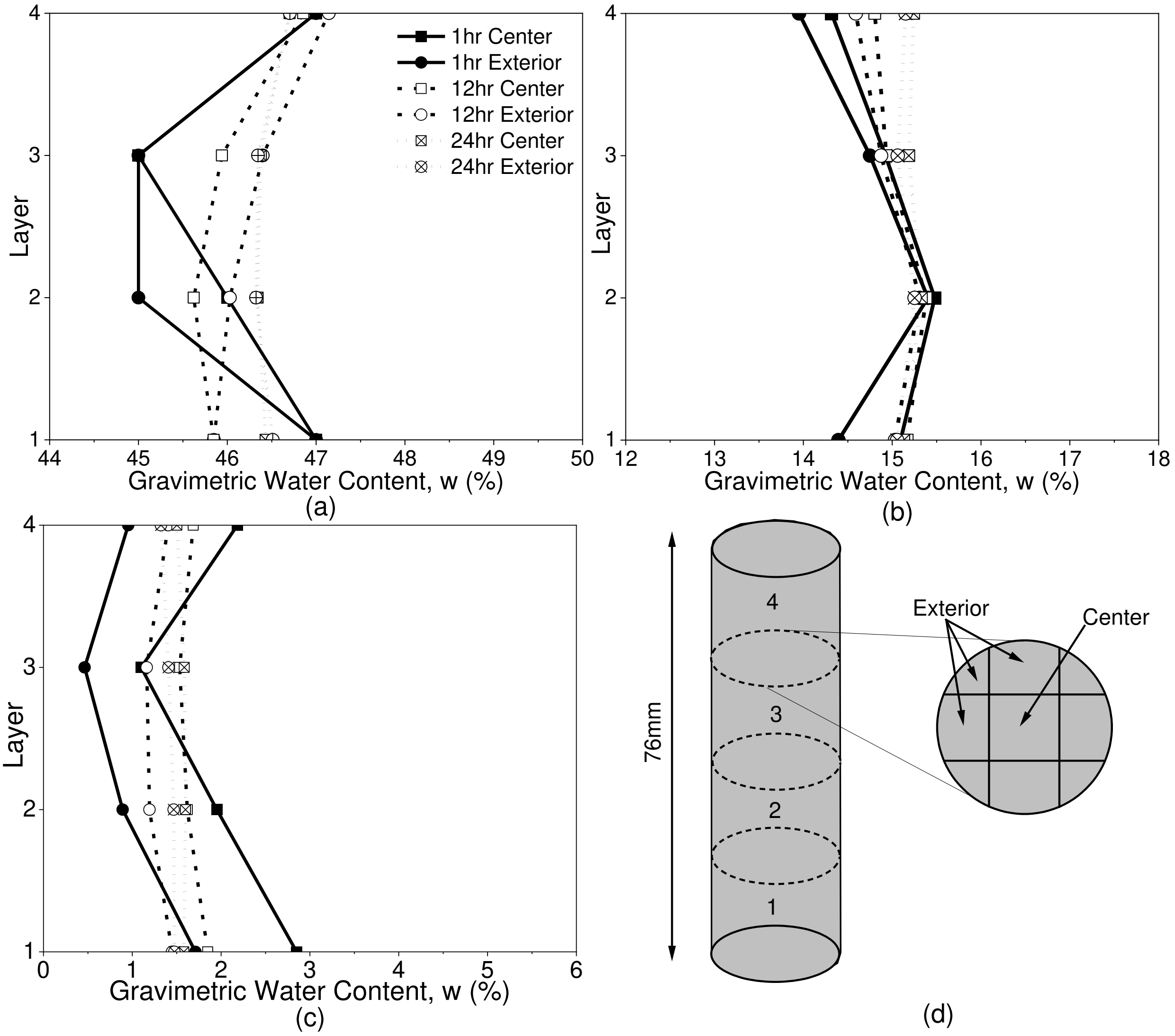

Figure 7. Water content distribution for kaolin after 1hr, 12hr and 24hr equilibration time for (a) full saturation, (b) drying to 15% water content, (c) drying to 1% water content and (d) layer positions and layer divisions.

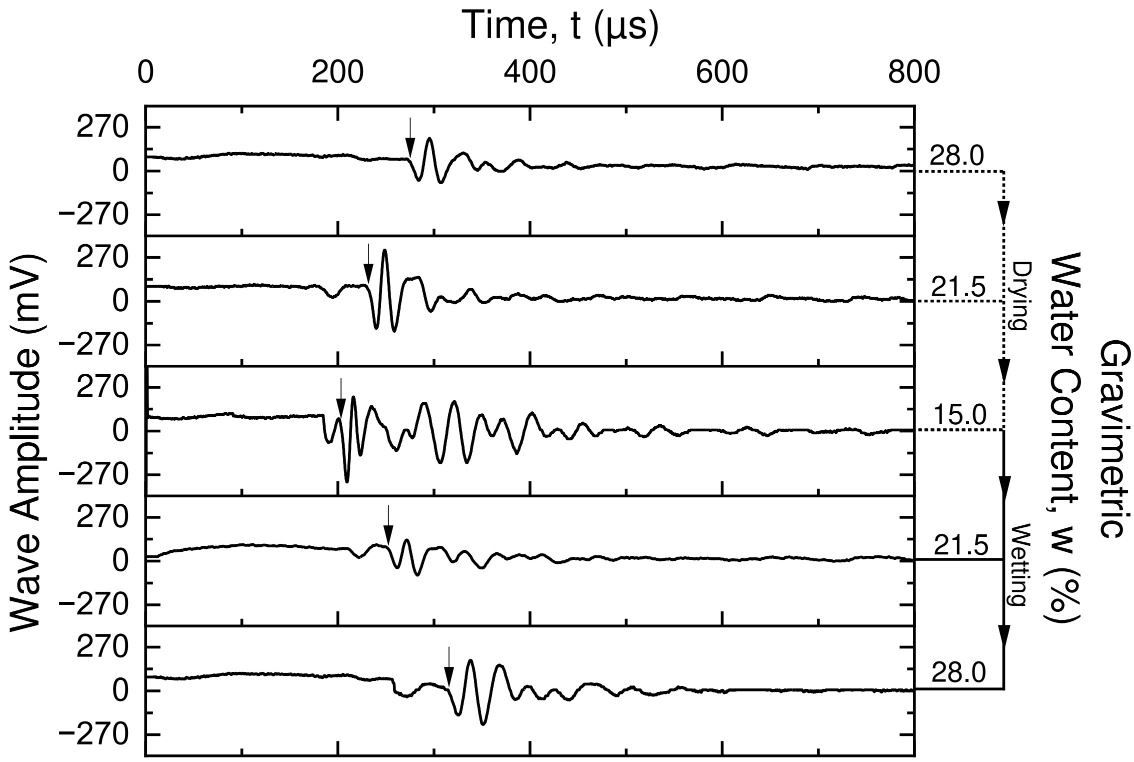

Figure 8. Typical shear wave trace evolution in time domain during drying and wetting cycle, arrows indicate interpretation of shear wave arrival time.

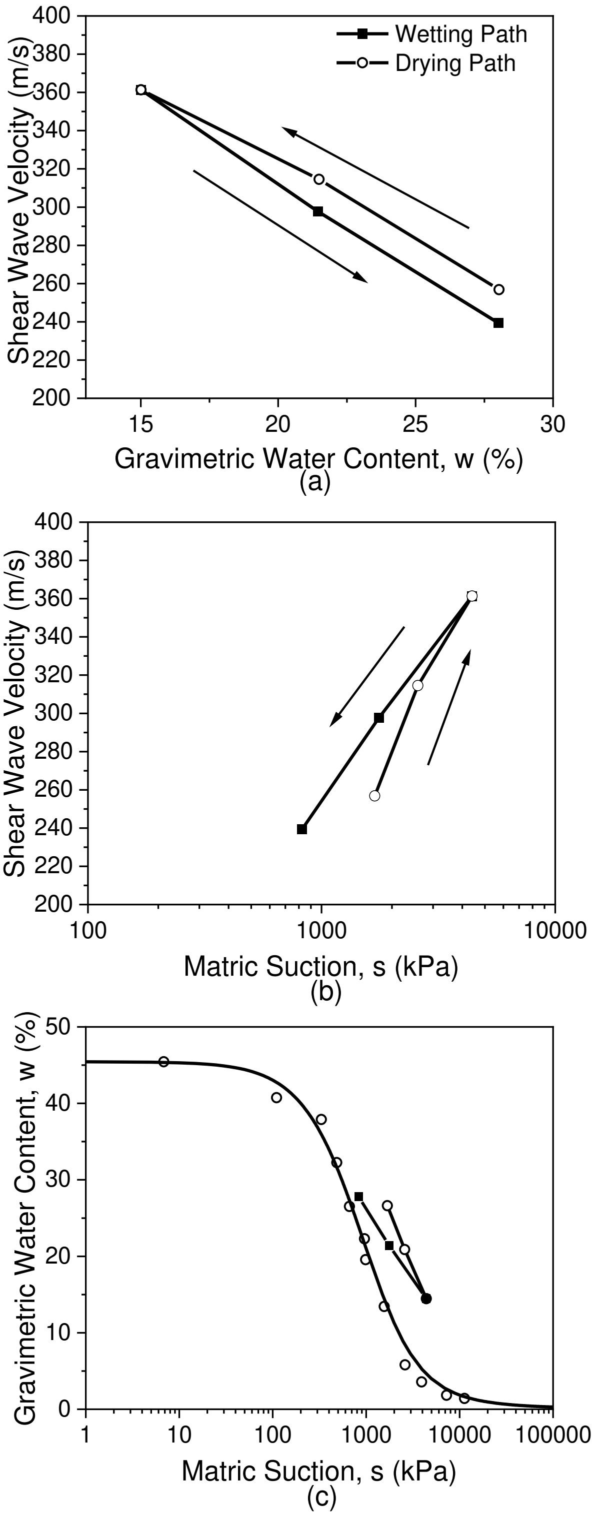

Figure 9. Shear wave velocity data for single drying-wetting path (CT) measured at constant water content, presented using variables a) gravimetric water content, b) matric suction and c) suction data and main drying SWRC.

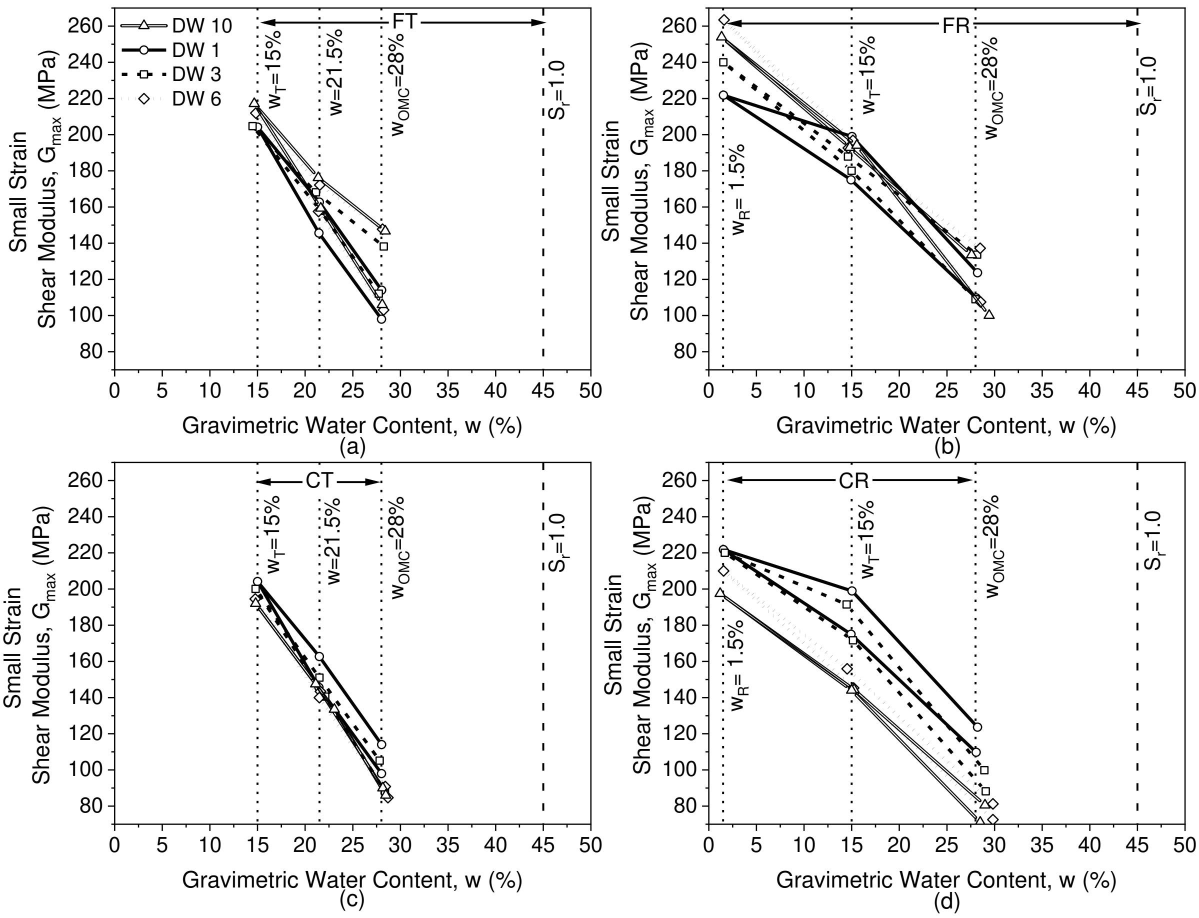

Figure 10. Small strain shear modulus of compacted kaolin specimens subjected to D/W 1, 3, 6, and 10 for a) FT - full saturation to transition zone, b) FR - full saturation to residual conditions, c) CT - compacted OMC to transition zone and d) CR – compacted OMC to residual conditions (note the arrows indicate the extent of drying-wetting cycles).

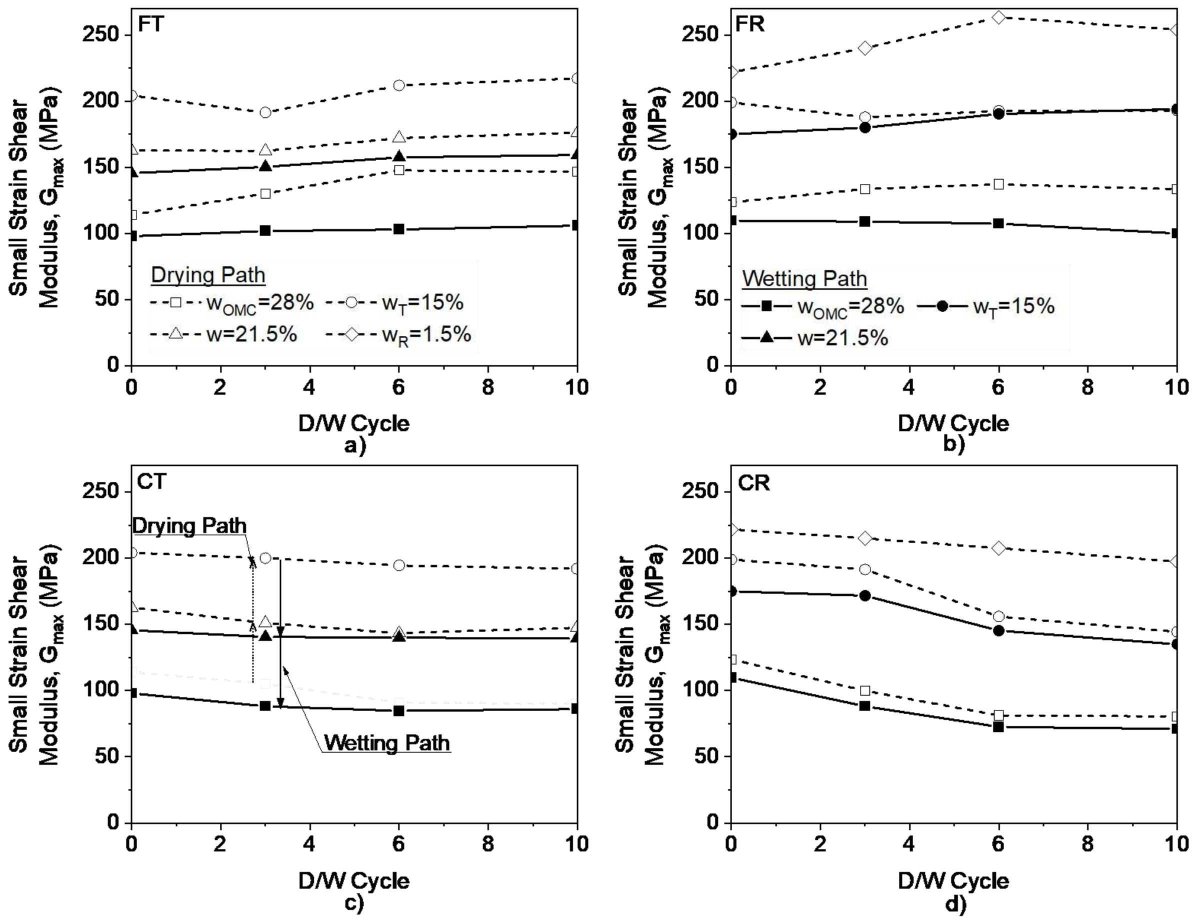

Figure 11. Small strain shear modulus of compacted kaolin specimens subjected to D/W 1, 3, 6, and 10 for a) FT - full saturation to transition zone, b) FR - full saturation to residual conditions, c) CT - compacted OMC to transition zone and d) CR – compacted OMC to residual conditions.

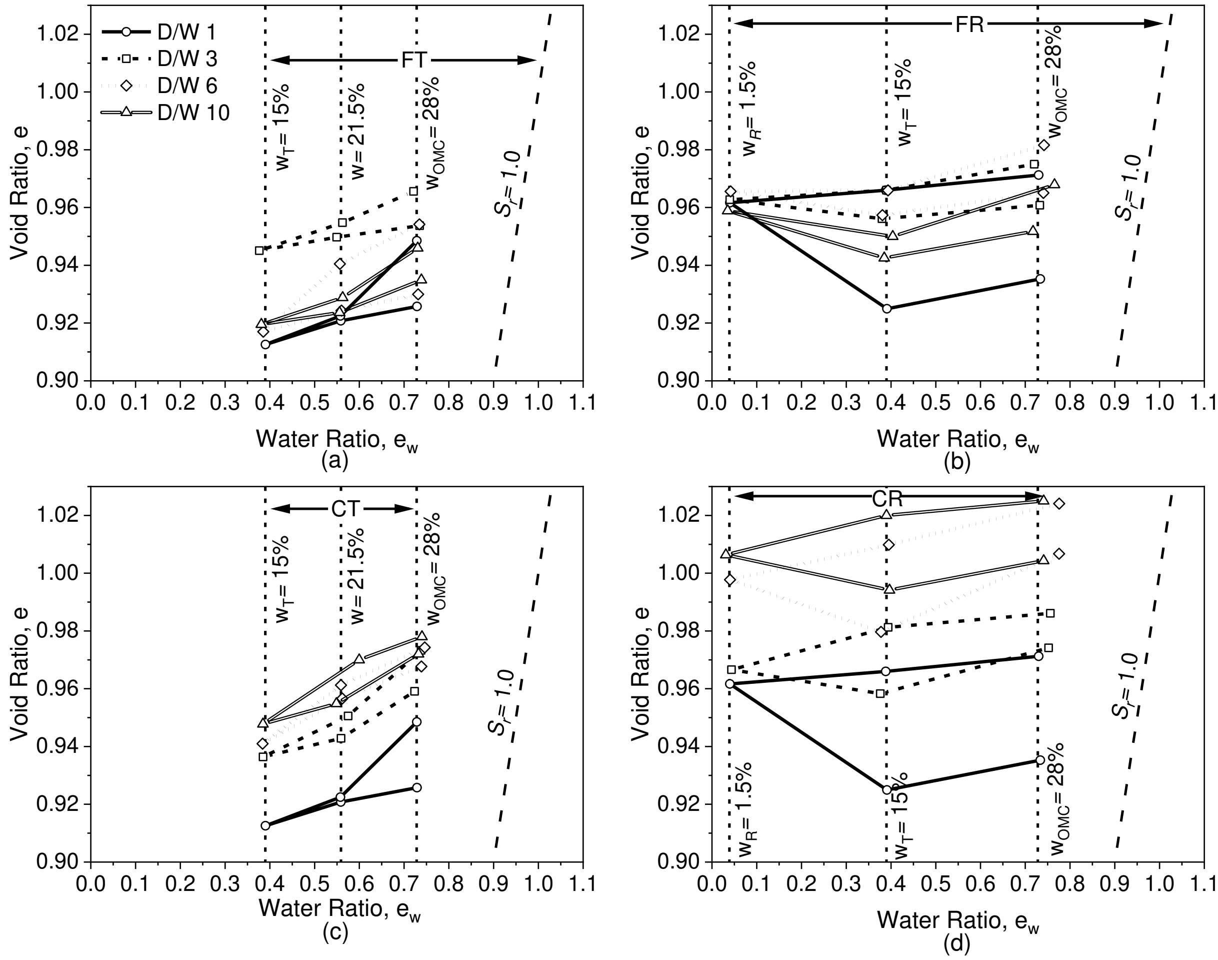

Figure 12. Volume change of compacted kaolin specimens subjected to D/W 1, 3, 6, and 10 for a) FT - full saturation to transition zone, b) FR - full saturation to residual conditions, c) CT - compacted OMC to transition zone, d) CR – compacted OMC to residual conditions (note the arrows indicate the extent of drying-wetting cycles).

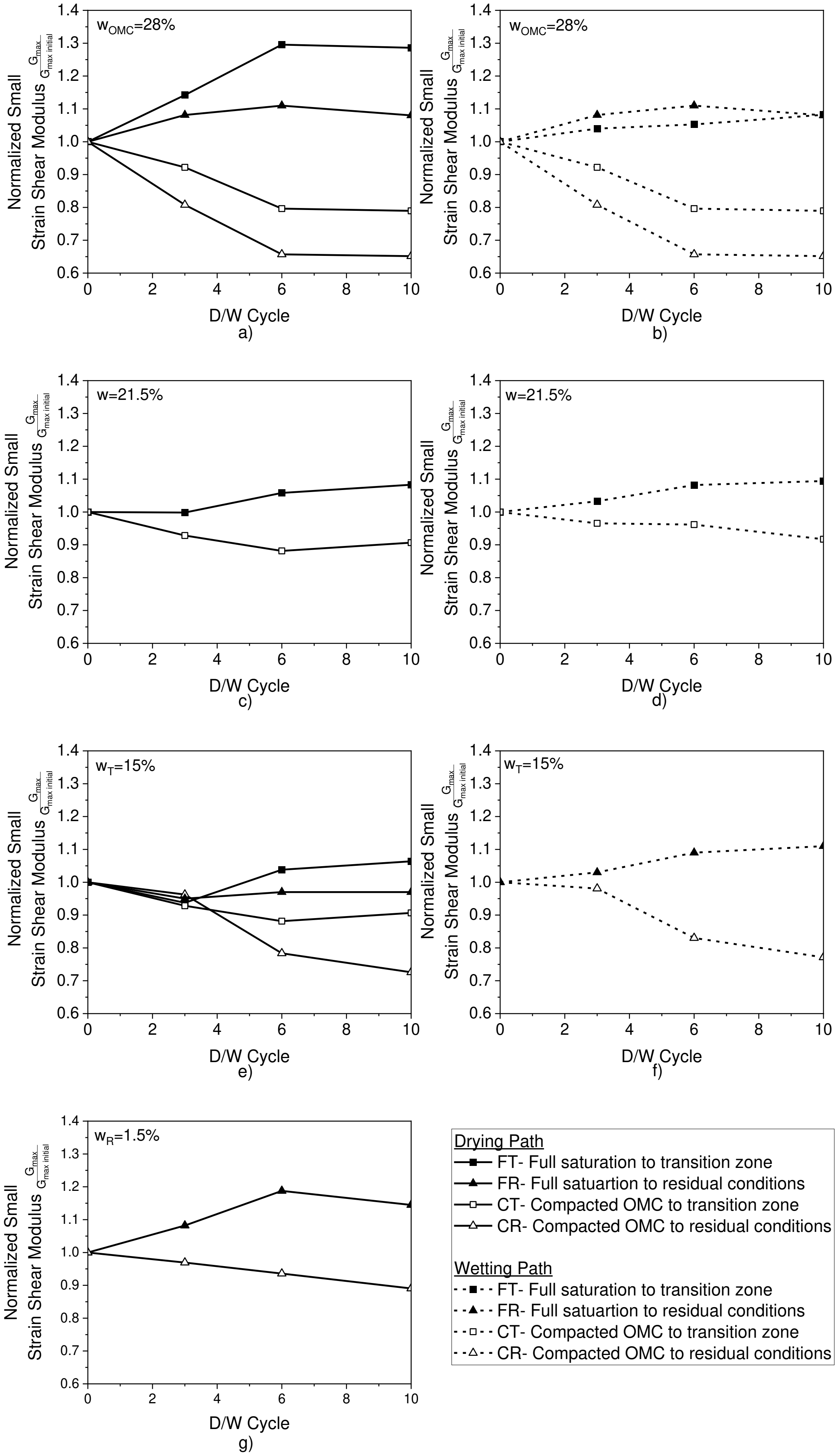

Normalized Small Strain Shear Modulus $\frac{G_{max}}{G_{max\ initial}}$
D/W Cycle
w_{OMC}=28%
a)
b)
w=21.5%
c)
d)
w_T=15%
e)
f)
w_R=1.5%
g)
Drying Path
FT- Full saturation to transition zone
FR- Full satuartion to residual conditions
CT- Compacted OMC to transition zone
CR- Compacted OMC to residual conditions
Wetting Path
FT- Full saturation to transition zone
FR- Full satuartion to residual conditions
CT- Compacted OMC to transition zone
CR- Compacted OMC to residual conditions

Figure 13. Normalized small strain shear modulus of compacted kaolin specimens at constant water content levels during drying-wetting cycles, for amplitudes: a) FT - full saturation to transition zone, b) FR - full saturation to residual conditions, CT - compacted OMC to transition zone and d) CR - compacted OMC to residual conditions.

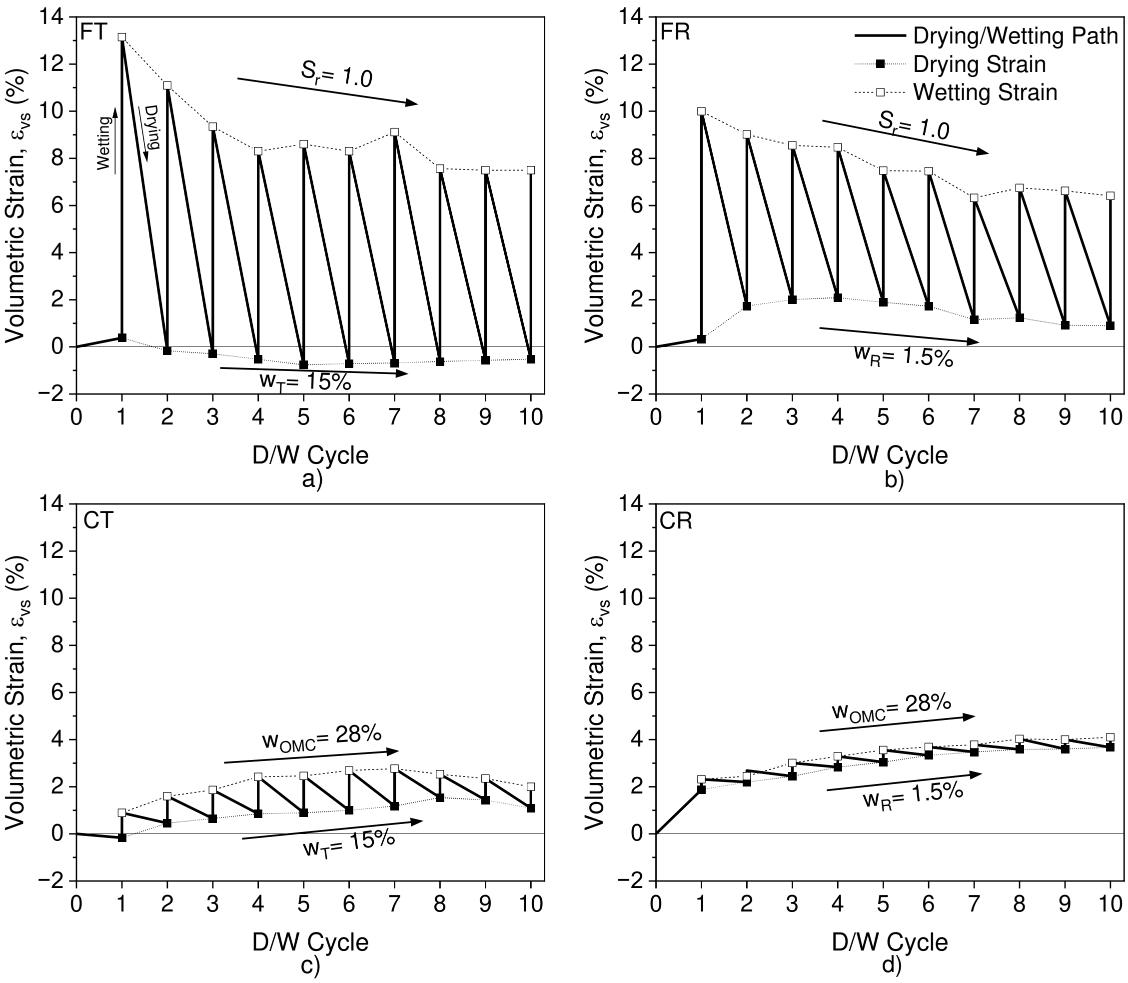

Figure 14. Volumetric strain at drying and wetting boundaries during the application of 10 cycles for a) FT - full saturation to transition zone, b) FR - full saturation to residual conditions, c) CT - compacted OMC to transition zone and d) CR - compacted OMC to residual conditions (compressive strains considered negative).

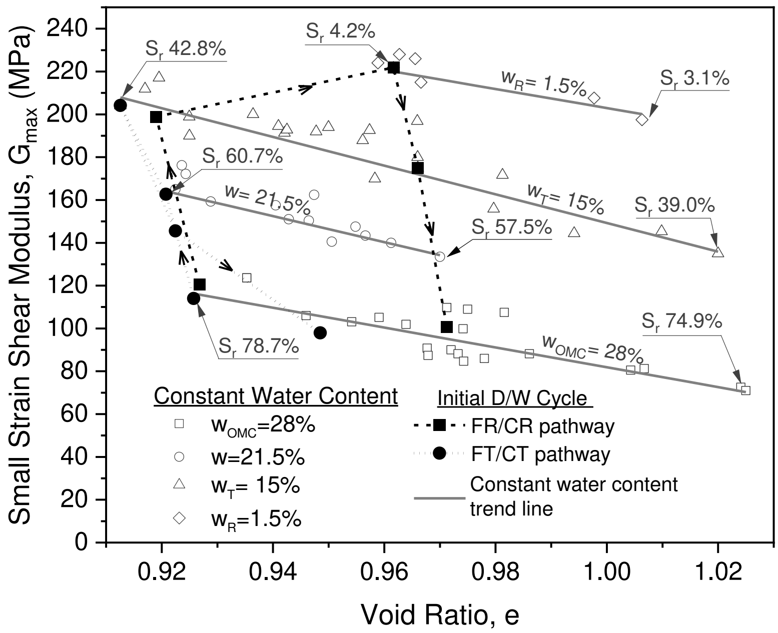

Figure 15. Relationship between void ratio and small strain shear modulus at constant water content for compacted kaolin subject to 10 drying and wetting cycles for all boundary conditions (FT/FR/CT/CR).